Random noise and pole dynamics in unstable front propagation

Zeev Olami, Barak Galanti, Oleg Kupervasser, and Itamar Procaccia
Department of Chemical Physics, The Weizmann Institute of Science, Rehovot 76 100, Israel
(Received 10 July 1996)

The problem of flame propagation is studied as an example of unstable fronts that wrinkle on many scales. The analytic tool of pole expansion in the complex plane is employed to address the interaction of the unstable growth process with random initial conditions and perturbations. We argue that the effect of random noise is immense and that it can never be neglected in sufficiently large systems. We present simulations that lead to scaling laws for the velocity and acceleration of the front as a function of the system size and the level of noise, and analytic arguments that explain these results in terms of the noisy pole dynamics.
[S1063-651X(97)01402-5]

PACS number(s): 47.27.Gs, 47.27.Jv, 05.40.+j

I. INTRODUCTION

The aim of this paper is to examine the role of random fluctuations on the dynamics of growing wrinkled interfaces that are governed by nonlinear equations of motion. We are interested in those examples for which the growth of a flat or smooth interface is inherently unstable. A famous example of such growth phenomena is provided by Laplacian growth patterns [1–3]. The experimental realization of such patterns is seen, for example, in Hele-Shaw cells [1] in which air or another low-viscosity fluid is displacing oil or some other high-viscosity fluid. Under normal conditions the advancing fronts do not remain flat; in channel geometries they form in time a stable finger whose width is determined by delicate effects that arise from the existence of surface tension. In radial geometry, the growth of the interface forms a contorted and ramified fractal shape. A related phenomenon has been studied in a model equation for flame propagation that has the same linear stability properties as the Laplacian growth problem [4]. The physical problem in this case is that of premixed flames that exist as self-sustaining fronts of exothermic chemical reactions in gaseous combustion. Experiments [5] on flame propagation in radial geometry show that the flame front accelerates as time goes on and roughens with characteristic exponents. Both observations did not receive proper theoretical explanations. It is notable that the channel and radial growth are markedly different; the former leads to a single giant cusp in the moving front, whereas the latter exhibits infinitely many cusps that appear in a complex hierarchy as the flame front develops [6,7].

Analytic techniques to study such processes are available [8]. In the context of flame propagation [7,9–11] and in Laplacian growth in the zero surface-tension limit [12–14] one can examine solutions that are described in terms of poles in the complex plane. This description is very useful in providing a set of ordinary differential equations for the positions of the poles, from which one can deduce the geometry of the developing front in an extremely economical and efficient way. Unfortunately, this description is not available in the case of Laplacian growth with surface tension and this makes the flame propagation problem very attractive. However, it suffers from one fundamental drawback. For the noiseless equation the pole dynamics always conserves the number of poles that existed in the initial conditions. As a result, there is a final degree of ramification that is afforded by every set of initial conditions even in the radial geometry and it is not obvious how to describe the continuing self-similar growth that is seen in experimental conditions or numerical simulations. Furthermore, as mentioned before, at least in the case of flame propagation, one observes [5] an *acceleration* of the flame front with time. Such a phenomenon is impossible when the number of poles is conserved. It is therefore tempting to conjecture that noise may have an important role in affecting the actual growth phenomena that are observed in such systems. In fact, the effect of noise on unstable front dynamics has not been adequately addressed in the literature. From the point of view of analytic techniques, noise can certainly generate new poles even if the initial conditions had a finite number of poles. The subject of pole dynamics with the existence of random noise and the interaction between random fluctuations and deterministic front propagation are the main issues of this paper.

We opt to study the example of flame propagation rather than Laplacian growth simply because the former has an analytic description in terms of poles also in the experimentally relevant case of finite viscosity. We choose to limit the present study to channel geometry. The reason is that in radial geometry it is more difficult to disentangle the effects of external noise from those of initial conditions. After all, initially the system can contain infinitely many poles, very far away near infinity in the complex plane (and therefore having an infinitely small contribution to the interface). Since the growth of the radius changes the stability of the system, more and more of these poles might fall down to the real axis and become observable. In channel geometry the analysis of the effect of initial conditions is relatively straightforward and one can understand it before focusing on the (more interesting) effects of external noise [9]. The basic reason for this is that in this geometry the noiseless steady-state solution for the developed front is known analytically. As described in Sec. II, in a channel of width L the steady-state solution is given in terms of $N(L)$ poles that are organized on a line parallel to the imaginary axis. It can be shown that for any number of poles in the initial conditions this is the only attractor of the pole dynamics. After the establishment of this steady state we can begin to systematically examine

the effects of external noise on this solution. As stated before, in radial conditions there is no stable steady state with a finite number of poles and the disentanglement of initial versus external perturbations is less straightforward [7]. We believe, nevertheless, that the insights provided in this paper have relevance for radial growth as well, as will be discussed in Sec. VI and in forthcoming papers.

We have a number of goals in this paper. First, after introducing the pole decomposition, the pole dynamics, and the basic steady state, we will present a stability analysis of the solutions of the flame propagation problem in a channel geometry. It will be shown that the giant cusp solution is linearly stable, but nonlinearly unstable. These results, which are described in Sec. III, can be obtained either by linearizing the dynamics around the giant cusp solutions in order to study the stability eigenvalues or by examining perturbations in the form of poles in the complex plane. The main result of Sec. III is that there exists one Goldstone mode and two modes whose eigenvalues hit the real axis periodically when the system size L increases. Thus the system is marginally stable at particular values of L and it is always nonlinearly unstable, allowing finite-size perturbations to introduce new poles into the system. This insight allows us to understand the relation between the system size and the effects of noise. In Sec. IV we discuss the relaxation dynamics that ensues after starting the system with ''small'' initial data. We study the coarsening process that leads in time to the final solution of the giant cusp and understand from this what the typical time scales are that exist in our dynamics. We offer in this section some results of numerical simulations that are interpreted in the later sections. In Sec. V we focus on the phenomenon of acceleration of the flame front and its relation to the existence of noise. In noiseless conditions the velocity of the flame front in a finite channel is bounded [9]. This can be shown either by using the pole dynamics or directly from the equation of motion. We will present the results of numerical simulations where the noise is controlled and show how the velocity of the flame front is affected by the level of the noise and the system size. The main results are the following. (i) Noise is responsible for introducing new poles to the system. (ii) For low levels of noise the velocity of the flame front scales with the system size with a characteristic exponent. (iii) There is a phase transition at a sharp (but system-size-dependent) value of the noise level, after which the behavior of the system changes qualitatively. (iv) After the phase transition the velocity of the flame front changes very rapidly with the noise level. In Sec. VI we remark on the implications of these observations for the scaling behavior of the radial growth problem and present a summary and conclusions.

II. EQUATIONS OF MOTION AND POLE DECOMPOSITION IN THE CHANNEL GEOMETRY

It is known that planar flames freely propagating through initially motionless homogeneous combustible mixtures are intrinsically unstable. It was reported that such flames develop characteristic structures that include cusps and under usual experimental conditions the flame front accelerates as time goes on. A model in $1+1$ dimensions that pertains to the propagation of flame fronts in channels of width $\tilde{L}$ was proposed in [4]. It is written in terms of position $h(x,t)$ of the flame front above the x axis. After appropriate rescalings it takes the form

$$\frac{\partial h(x,t)}{\partial t}=\frac{1}{2}\left[\frac{\partial h(x,t)}{\partial x}\right]^2+\nu\frac{\partial^2 h(x,t)}{\partial x^2}+I\{h(x,t)\}+1. \tag{1}$$

The domain is $0<x<\tilde{L}$, ν is a parameter, and we use periodic boundary conditions. The functional $I[h(x,t)]$ is the Hilbert transform, which is conveniently defined in terms of the spatial Fourier transform

$$h(x,t)=\int_{-\infty}^{\infty}e^{ikx}\hat{h}(k,t)dk, \tag{2}$$

$$I[h(k,t)]=|k|\hat{h}(k,t). \tag{3}$$

For the purpose of introducing the pole decomposition it is convenient to rescale the domain to $0<\theta<2\pi$. Performing this rescaling and denoting the resulting quantities with the same notation we have

$$\frac{\partial h(\theta,t)}{\partial t}=\frac{1}{2L^2}\left[\frac{\partial h(\theta,t)}{\partial \theta}\right]^2+\frac{\nu}{L^2}\frac{\partial^2 h(\theta,t)}{\partial \theta^2}+\frac{1}{L}I\{h(\theta,t)\}+1. \tag{4}$$

In this equation $L=\tilde{L}/2\pi$. Next we change variables to $u(\theta,t)\equiv\partial h(\theta,t)/\partial\theta$. We find

$$\frac{\partial u(\theta,t)}{\partial t}=\frac{u(\theta,t)}{L^2}\frac{\partial u(\theta,t)}{\partial \theta}+\frac{\nu}{L^2}\frac{\partial^2 u(\theta,t)}{\partial \theta^2}+\frac{1}{L}I\{u(\theta,t)\}. \tag{5}$$

It is well known that the flat front solution of this equation is linearly unstable. The linear spectrum in k representation is

$$\omega_k=|k|/L-\nu k^2/L^2. \tag{6}$$

There exists a typical scale $k_{\max}$ that is the last unstable mode

$$k_{\max}=\frac{L}{\nu}. \tag{7}$$

Nonlinear effects stabilize a new steady state, which is discussed next.

The outstanding feature of the solutions of this equation is the appearance of cusplike structures in the developing fronts. Therefore, a representation in terms of Fourier modes is very inefficient. Rather, it appears very worthwhile to represent such solutions in terms of sums of functions of poles in the complex plane. It will be shown below that the position of the cusp along the front is determined by the real coordinate of the pole, whereas the height of the cusp is in correspondence with the imaginary coordinate. Moreover, it will be seen that the dynamics of the developing front can be usefully described in terms of the dynamics of the poles. Following [8,9,11,7], we expand the solutions $u(\theta,t)$ in functions that depend on N poles whose position $z_j(t)\equiv x_j(t)+iy_j(t)$ in the complex plane is time dependent:

$$u(\theta,t)=\nu\sum_{j=1}^{N}\cot\left[\frac{\theta-z_j(t)}{2}\right]+\text{c.c.}$$
$$=\nu\sum_{j=1}^{N}\frac{2\sin[\theta-x_j(t)]}{\cosh[y_j(t)]-\cos[\theta-x_j(t)]}, \tag{8}$$

$$h(\theta,t)=2\nu\sum_{j=1}^{N}\ln\{\cosh[y_j(t)]-\cos[\theta-x_j(t)]\}+C(t). \tag{9}$$

In Eq. (9), $C(t)$ is a function of time. The function (9) is a superposition of quasicusps (i.e., cusps that are rounded at the tip). The real part of the pole position (i.e., x_j) is the coordinate (in the domain $[0,2\pi]$) of the maximum of the quasicusp and the imaginary part of the pole position (i.e., y_j) is related to the depth of the quasicusp. As y_j decreases the depth of the cusp increases. As $y_j\to 0$ the depth diverges to infinity. Conversely, when $y_j\to\infty$ the depth decreases to zero.

The main advantage of this representation is that the propagation and wrinkling of the front can be described via the dynamics of the poles. Substituting Eq. (8) in Eq. (5), we derive the following ordinary differential equations for the positions of the poles:

$$-L^2\frac{dz_j}{dt}=\left[\nu\sum_{k=1,k\neq j}^{2N}\cot\left(\frac{z_j-z_k}{2}\right)+i\frac{L}{2}\text{sgn}[\text{Im}(z_j)]\right]. \tag{10}$$

We note that in Eq. (8), due to the complex conjugation, we have $2N$ poles that are arranged in pairs such that for $j<N$, $z_{j+N}=\overline{z_j}$. In the second sum in Eq. (8) each pair of poles contributed one term. In Eq. (10) we again employ $2N$ poles since all of them interact. We can write the pole dynamics in terms of the real and imaginary parts x_j and y_j. Because of the arrangement in pairs it is sufficient to write the equation for either $y_j>0$ or $y_j<0$. We opt for the first. The equations for the positions of the poles read

$$-L^2\frac{dx_j}{dt}=\nu\sum_{k=1,k\neq j}^{N}\sin(x_j-x_k)\{[\cosh(y_j-y_k)-\cos(x_j-x_k)]^{-1}+[\cosh(y_j+y_k)-\cos(x_j-x_k)]^{-1}\}, \tag{11}$$

$$L^2\frac{dy_j}{dt}=\nu\sum_{k=1,k\neq j}^{N}\left(\frac{\sinh(y_j-y_k)}{\cosh(y_j-y_k)-\cos(x_j-x_k)}+\frac{\sinh(y_j+y_k)}{\cosh(y_j+y_k)-\cos(x_j-x_k)}\right)+\nu\coth(y_j)-L. \tag{12}$$

We note that if the initial conditions of the differential equation (5) are expandable in a finite number of poles, these equations of motion preserve this number as a function of time. On the other hand, this may be an unstable situation for the partial differential equation and noise can change the number of poles. This issue will be examined at length in Sec. V. We turn now to a discussion of the steady-state solution of the equations of the pole dynamics.

Qualitative properties of the stationary solution

The steady-state solution of the flame front propagating in channels of width 2π was presented in Ref. [9]. Using these results, we can immediately translate the discussion to a channel of width L. The main results are summarized as follows.

(i) There is only one stable stationary solution that is geometrically represented by a giant cusp (or, equivalently, one finger) and analytically by $N(L)$ poles that are aligned on one line parallel to the imaginary axis. The existence of this solution is made clearer with the following remarks.

(ii) There exists an attraction between the poles along the real line. This is obvious from Eq. (11), in which the sign of dx_j/dt is always determined by $\sin(x_j-x_k)$. The resulting dynamics merges all the x positions of poles whose y position remains finite.

(iii) The y positions are distinct and the poles are aligned above each other in positions $y_{j-1}<y_j<y_{j+1}$ with the maximal being $y_{N(L)}$. This can be understood from Eq. (12), in which the interaction is seen to be repulsive at short ranges, but changes sign at longer ranges.

(iv) If one adds an additional pole to such a solution, this pole (or another) will be pushed to infinity along the imaginary axis. If the system has less than $N(L)$ poles it is unstable to the addition of poles and any noise will drive the system towards this unique state. The number $N(L)$ is

$$N(L)=\left[\frac{1}{2}\left(\frac{L}{\nu}+1\right)\right], \tag{13}$$

where [ ] is the integer part. To see this consider a system with N poles and such that all the values of y_j satisfy the condition $0<y_j<y_{\max}$. Add now one additional pole whose coordinates are $z_a\equiv(x_a,y_a)$ with $y_a\gg y_{\max}$. From the equation of motion for y_a [Eq. (12)] we see that the terms in the sum are all of the order of unity, as is the $\cot(y_a)$ term. Thus the equation of motion of y_a is approximately

$$\frac{dy_a}{dt}\approx\nu\frac{2N+1}{L^2}-\frac{1}{L}. \tag{14}$$

The fate of this pole depends on the number of other poles. If N is too large the pole will run to infinity, whereas if N is small the pole will be attracted towards the real axis. The condition for moving away to infinity is that $N>N(L)$, where $N(L)$ is given by Eq. (13). On the other hand, the y coordinate of the poles cannot hit zero. Zero is a repulsive line and poles are pushed away from zero with infinite velocity. To see this consider a pole whose y_j approaches zero. For any finite L the term $\coth(y_j)$ grows unboundedly, whereas all the other terms in Eq. (12) remain bounded.

(v) The height of the cusp is proportional to L. The distribution of positions of the poles along the line of constant x was worked out in [9].

We will refer to the solution with all these properties as the Thual-Frisch-Hénon (TFH) cusp solution. Next we turn to the stability analysis of this solution.

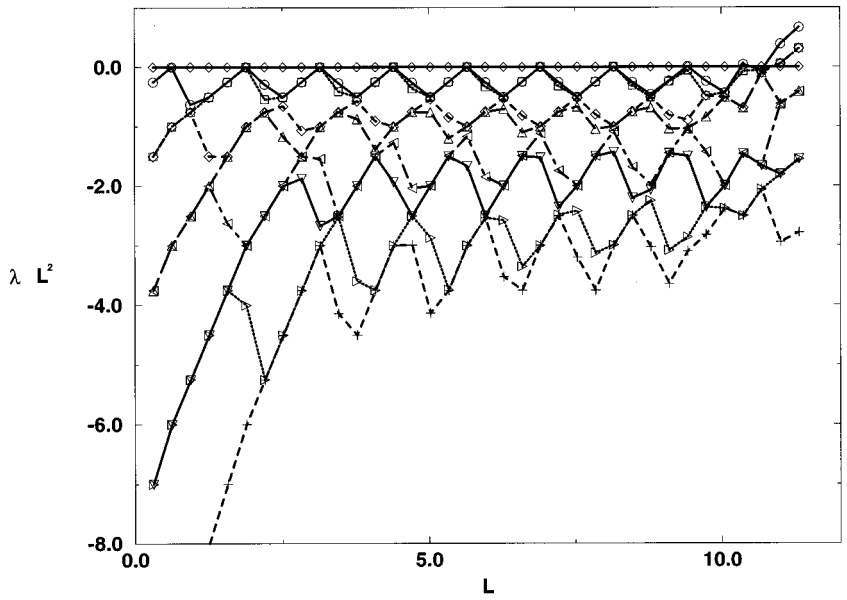

FIG. 1. First ten highest eigenvalues of the stability matrix with $\nu=1$, multiplied by the square of the system size L^2 vs the system size L. Note that all the eigennvalues oscillate around fixed values in this presentation and that the highest two eigenvalues hit zero periodically.

III. LINEAR STABILITY ANALYSIS IN CHANNEL GEOMETRY

In this section we discuss the linear stability of the TFH cusp solution. To this aim we first use Eq. (8) to write the steady solution $u_s(\theta)$ in the form

$$u_s(\theta)=\nu\sum_{j=1}^{N}\frac{2\sin[\theta-x_s]}{\cosh[y_j]-\cos[\theta-x_s]}, \tag{15}$$

where x_s is the real (common) position of the stationary poles and y_j their stationary imaginary position. To study the stability of this solution we need to determine the actual positions y_j. This is done numerically by integrating the equations of motion for the poles starting from N poles in initial positions and waiting for relaxation. Next one perturbs this solution with a small perturbation $\phi(\theta,t)$: $u(\theta,t)=u_s(\theta)+\phi(\theta,t)$. Linearizing the dynamics for small ϕ results in the equation of motion

$$\frac{\partial\phi(\theta,t)}{\partial t}=\frac{1}{L^2}\{\partial_\theta[u_s(\theta)\phi(\theta,t)]+\nu\partial_\theta^2\phi(\theta,t)\}+\frac{1}{L}I(\phi(\theta,t)). \tag{16}$$

A. Fourier decomposition and eigenvalues

The linear equation can be decomposed in Fourier modes according to

$$\phi(\theta,t)=\sum_{k=-\infty}^{\infty}\hat{\phi}_k(t)e^{ik\theta}, \tag{17}$$

$$u_s(\theta)=-2\nu i\sum_{k=-\infty}^{\infty}\sum_{j=1}^{N}\mathrm{sgn}(k)e^{-|k|y_j}e^{ik\theta}. \tag{18}$$

In these sums the discrete k values run over all the integers. Substituting in Eq. (16), we get the equations

$$\frac{d\hat{\phi}_k(t)}{dt}=\sum_n a_{kn}\hat{\phi}_n(t), \tag{19}$$

where a_{kn} is an infinite matrix whose entries are given by

$$a_{kk}=\frac{|k|}{L}-\frac{\nu}{L^2}k^2, \tag{20}$$

$$a_{kn}=\frac{k}{L^2}\mathrm{sgn}(k-n)\left(2\nu\sum_{j=1}^{N}e^{-|k-n|y_j}\right),\quad k\neq n. \tag{21}$$

To solve for the eigenvalues of this matrix we need to truncate it at some cutoff k vector k^*. The choice of k^* can be based on the linear stability analysis of the flat front. The scale $k_{\max}$ [cf. Eq. (7)] is the largest k that is still linearly unstable. We must choose $k^*>k_{\max}$ and test the choice by the converegence of the eigenvalues. The chosen value of k^* in our numerics was $4k_{\max}$. The results for the low-order eigenvalues of the matrix a_{kn} that were obtained from a converged numerical calculation are presented in Fig. 1. The eigenvalues are multiplied by L^2 and are plotted as a function of L. We order the eigenvalues in decreasing order and denote them as $\lambda_0\leqslant\lambda_1\leqslant\lambda_2\leqslant\cdots$. The figure offers a number of qualitative observations.

(i) There exists an obvious Goldstone or translational mode $u_s'(\theta)$ with eigenvalue $\lambda_0=0$, which is shown with rhombuses in Fig. 1. This eigenmode stems from the Galilean invariance of the equation of motion.

(ii) The eigenvalues oscillate periodically between values that are L independent in this presentation (in which we multiply by L^2). In other words, up to the oscillatory behavior the eigenvalues depend on L like L^{-2}.

(iii) The eigenvalues λ_1 and λ_2, which are represented by squares and circles in Fig. 1, hit zero periodically. The functional dependence in this presentation appears almost piecewise linear.

(iv) The higher eigenvalues also exhibit similar qualitative behavior, but without reaching zero. We note that the solution becomes marginally stable for every value of L for

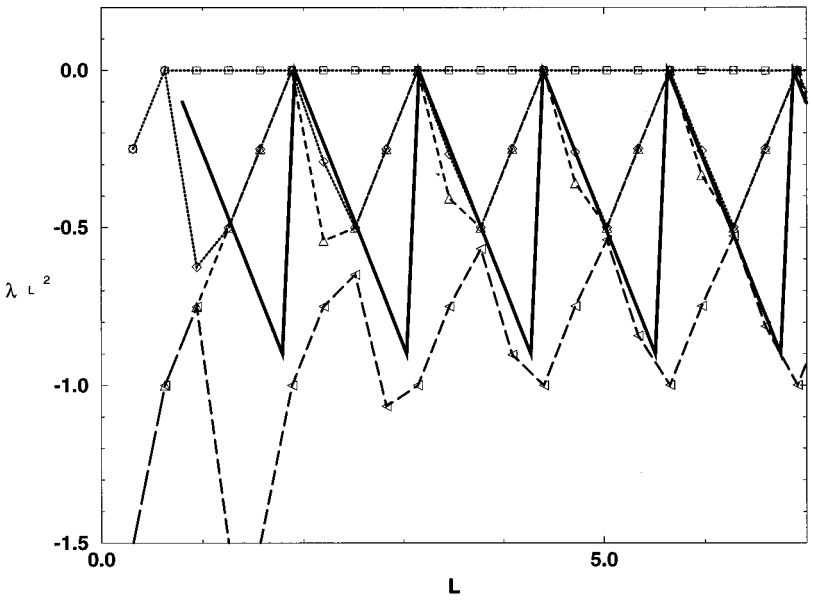

FIG. 2. Comparison of the numerically determined, highest four eigenvalues of the stability matrix with the prediction of the pole analysis. The eigenvalues of the stability matrix are λ_0 (squares), λ_1 (rhombuses), λ_2 (triangles), and λ_3 (slanted triangles). The pole analysis (solid line) provides a qualitative understanding of the stability and appears to overlap with the highest eigenvector over half of the range and with the fourth eigenvalue over the other half.

which the eigenvalues λ_1 and λ_2 hit zero. The L^{-2} dependence of the spectrum indicates that the solution becomes more and more sensitive to noise as L increases.

B. Qualitative understanding using pole analysis

The most interesting qualitative aspects are those enumerated above as items (ii) and (iii). To understand them it is useful to return to the pole description, and to focus on Eq. (14). This equation describes the dynamics of a single faraway pole. We remarked before that this equation shows that for *fixed* L the stable number of poles is the integer part (13). Define now the number α, $0 \leqslant \alpha \leqslant 1$, according to

$$\alpha = \left[\frac{1}{2}\left(\frac{L}{\nu}+1\right)\right] - \frac{1}{2}\left(\frac{L}{\nu}-1\right). \tag{22}$$

Using this number we rewrite Eq. (14) as

$$\frac{dy_a}{dt} \approx \frac{2\nu}{L^2}\alpha. \tag{23}$$

As L increases, α oscillates piecewise linearly and periodically between zero and unity. This shows that a distant pole that is added to the giant cusp solution is usually repelled to infinity except when α hits zero and the system becomes marginally unstable to the addition of a new pole.

To connect this to the linear stability analysis we note from Eq. (8) that a single faraway pole solution (i.e., with y very large) can be written as

$$u(\theta,t) = 4\nu e^{-y(t)} \sin[\theta - x(t)]. \tag{24}$$

Suppose that we add to our giant cusp solution a perturbation of this functional form. From Eq. (23) we know that y grows linearly in time and therefore this solution decays exponentially in time. The rate of decay is a linear eigenvalue of the stability problem and from Eq. (23) we understand both the $1/L^2$ dependence and the periodic marginality. We should note that this way of thinking gives us a significant part of the L dependence of the eigenvalues, but not all. The variable α is rising from zero to unity periodically, but after reaching unity it hits zero instantly. Accordingly, if the highest nonzero eigenvalue were fully determined by the pole analysis, we would expect this eigenvalue to behave as the solid line shown in Fig. 2. The actual highest eigenvalue computed from the stability matrix is shown in rhombuses connected by dotted line. It is clear that the pole analysis gives us a great deal of qualitative and quantitative understanding, but not all the features agree.

C. Dynamics near marginality

The discovery of marginality at isolated values of L poses questions regarding the fate of poles that are added at very large y's at certain x positions. We will argue now that when the system becomes marginally stable, a new pole can be added to those existing in the giant cusp. We remember that these poles have a common θ position that we denote as $\theta = \theta_c$. The fate of a new pole added at infinity depends on its θ position. If the position of the new pole is again denoted as y_a and $\infty \gg y_a \gg y_{\max}$, we can see from Eq. (12) that dy_a/dt is maximal when $\theta_a = \theta_c$, whereas it is minimal when $\theta_a - \theta_c = \pi$. This follows from the fact that the cosine term has a value $+1$ when $\theta_a = \theta_c$ and a value -1 when $\theta_a - \theta_c = \pi$. For large-$y$ differences the terms in the sum take on their minimal value when the cosine term is -1 and their maximal values at $+1$. For infinitely large y_a the equation of motion is Eq. (14), which is independent of θ_a. Since the right-hand side of this equation becomes zero at marginality, we conclude that for very large but finite y_a, dy_a/dt changes sign from positive to negative when $\theta_a - \theta_c$ changes from zero to π. The meaning of this observation is that the most unstable points in the system are those points that are farthest away from the giant cusp. It is interesting to discuss the fate of a pole that is added to the system at such a position. From the point of view of the pole dynamics $\theta = \theta_c + \pi$ is an unstable fixed point for the motion along the θ axis. The attraction to the giant cusp exactly vanishes at this point. If we start with a pole at a very large y_a close to this value of θ the downfall along the y coordinate will be

faster than the lateral motion towards the giant cusp. We therefore expect to see the creation of a small cusp at θ values close to π that precedes a later stage of motion in which the small cusp moves to merge with the giant cusp. Upon the approach of the new pole to the giant cusp all the existing poles will move up and the farthest pole at $y_{\max}$ will be kicked off to infinity. We will later explain that this type of dynamics occurs in stable systems that are driven by noise. The noise generates far away poles (in the imaginary direction) that get attracted around $\theta=\theta_c+\pi$ to create small cusps that run continuously towards the giant cusp.

D. Nonlinear stability

The intuition gained so far can be used to discuss the issue of stability of a stable system to *larger* perturbations. In other words, we may want to add to the system poles at finite values of y and ask about their fate. We first show in this subsection that poles whose initial y value is below $y_{\max}\sim\ln(L^2/\nu^2)$ will be attracted towards the real axis. The scenario is similar to the one described in the preceding subsection.

Suppose that we generate a stable system with a giant cusp at $\theta_c=0$ with poles distributed along the y axis up to $y_{\max}$. We know that the sum of all the forces that act on the upper pole is zero. Consider then an additional pole inserted in the position $(\pi,y_{\max})$. It is obvious from Eq. (12) that the forces acting on this pole will pull it downward. On the other hand, if its initial position is much above $y_{\max}$ the force on it will be repulsive towards infinity. We see that this simple argument identifies $y_{\max}$ as the typical scale for nonlinear instability.

Next we estimate $y_{\max}$ and interpret our result in terms of the *amplitude* of a perturbation of the flame front. We explained that uppermost pole's position fluctuates between a minimal value and infinity as L is changing. We want to estimate the characteristic scale of the minimal value of $y_{\max}(L)$. To this aim we employ the result of Ref. [9] regarding the stable distribution of pole positions in a stable large system. The parametrization of [9] differs from ours; to go from our parametrization in Eq. (5) to theirs we need to rescale u by L^{-1} and t by L. The parameter ν in their parametrization is ν/L in ours. According to [9], the number of poles between y and $y+dy$ is given by the $\rho(y)dy$, where the density $\rho(y)$ is

$$\rho(y)=\frac{L}{\pi^2\nu}\ln[\coth(|y|/4)]. \tag{25}$$

To estimate the minimal value of $y_{\max}$ we require that the tail of the distribution $\rho(y)$ integrated between this value and infinity will allow one single pole. In other words,

$$\int_{y_{\max}}^{\infty}dy\rho(y)\approx 1. \tag{26}$$

Expanding Eq. (25) for large y and integrating explicitly the result in Eq. (26), we end up with the estimate

$$y_{\max}\approx 2\ln\left[\frac{4L}{\pi^2\nu}\right]. \tag{27}$$

For large L this result is $y_{\max}\approx\ln(L^2/\nu^2)$. If we now add an additional pole in the position $(\theta,y_{\max})$ this is equivalent to perturbing the solution $u(\theta,t)$ with a function $\nu e^{-y_{\max}}\sin(\theta)$, as can be seen directly from Eq. (8). We thus conclude that the system is unstable to a perturbation *larger* than

$$u(\theta)\sim\nu^3\sin(\theta)/L^2. \tag{28}$$

This indicates a very strong size dependence of the sensitivity of the giant cusp solution to external perturbations. This will be an important ingredient in our discussion of noisy systems.

IV. INITIAL CONDITIONS, POLE DECOMPOSITION, AND COARSENING

In this section we show first that any initial conditions can be approximated by pole decomposition. Later we show that the dynamics of sufficiently smooth initial data can be well understood from the pole decomposition. Finally, we employ this picture to describe the *inverse cascade* of cusps into the giant cusp that is the final steady state. By inverse cascade we mean a nonlinear coarsening process in which the small scales coalesce in favor of larger scales and finally the system staturates at the largest available scale [16].

A. Pole expansion: General comments

The fundamental question is how many poles are needed to describe any given initial condition. The answer, of course, depends on how smooth are the initial conditions. Suppose also that we have an initial function $u(\theta,t=0)$ that is 2π periodic and at time $t=0$ admits a Fourier representation

$$u(\theta)=\sum_{k=1}^{\infty}A_k\sin(k\theta+\phi_k), \tag{29}$$

with $A_k>0$ for all k. Suppose that we want to find a pole-decomposition representation $u_p(\theta)$ such that

$$|u_p(\theta)-u(\theta)|\leqslant\epsilon \quad \text{for every } \theta, \tag{30}$$

where ϵ is a given wanted accuracy. If $u(\theta)$ is differentiable we can cut the Fourier expansion at some finite $k=K$ knowing that the remainder is smaller than, say, $\epsilon/2$. Choose now a large number M and a small number $\Delta\ll 1/M$ and write the pole representation for $u_p(\theta)$ as

$$u_p(\theta)=\sum_{k=1}^{K}\sum_{p=0}^{M-1}\frac{2k\,\sin(k\theta+\phi_k)}{\cosh[k(y_k+p\Delta)]-\cos(k\theta+\phi_k)}. \tag{31}$$

To see that this representation is a particular form of the general formula (8) we use the two identities

$$\sum_{k=0}^{\infty}e^{-kt}\sin xk=\frac{1}{2}\frac{\sin x}{\cosh t-\cos x}, \tag{32}$$

$$\sum_{k=0}^{K-1}\sin(x+ky)=\sin\left(x+\frac{K-1}{2}y\right)\sin\frac{Ky}{2}\csc\frac{y}{2}. \tag{33}$$

From these follows a third identity

$$\sum_{j=0}^{K-1} \frac{2\sin\left(x-\frac{2\pi j}{K}+\phi\right)}{\cosh y-\cos\left(x-\frac{2\pi j}{K}+\phi\right)} = \frac{2K\,\sin(Kx+\phi)}{\cosh Ky-\cos(Kx+\phi)}. \tag{34}$$

Note that the left-hand side of Eq. (34) is of the form (8) with K poles whose positions are all on the line $y_j=y$ and whose x_j are on the lattice points $2\pi j/K-\phi$. On the other hand, every term in Eq. (31) is of this form.

Next we use Eq. (32) to rewrite Eq. (31) in the form

$$u_p(\theta)=\sum_{k=1}^{K}\sum_{p=0}^{M-1}\sum_{n=1}^{\infty} 4ke^{-nk(y_k+p\Delta)}\sin(nk\theta+n\phi_k). \tag{35}$$

Exchanging the order of summation between n and p, we can perform the geometric sum on p. Denoting

$$b_{n,k}\equiv\sum_{p=0}^{M-1} e^{-nkp\Delta}=\frac{1-e^{-Mkn\Delta}}{1-e^{-kn\Delta}}, \tag{36}$$

we find

$$\begin{aligned} u_p(\theta)&=\sum_{k=1}^{K}\sum_{n=1}^{\infty} 4kb_{n,k}e^{-nky_k}\sin(nk\theta+n\phi_k)\\ &=\sum_{k=1}^{K}\sum_{n=2}^{\infty} 4kb_{n,k}e^{-nky_k}\sin(nk\theta+n\phi_k)\\ &\quad+\sum_{k=1}^{K} 4kb_{1,k}e^{-ky_k}\sin(k\theta+\phi_k). \end{aligned} \tag{37}$$

Compare now the second term on the right-hand side of Eq. (37) with Eq. (29). We can identify

$$e^{-ky_k}=\frac{A_k}{4kb_{1,k}}. \tag{38}$$

The first term can be then bound from above as

$$\begin{aligned} &\left|\sum_{k=1}^{K}\sum_{n=2}^{\infty} 4kb_{n,k}e^{-nky_k}\sin(nk\theta+n\phi_k)\right|\\ &\quad\leqslant\sum_{k=1}^{K}\sum_{n=2}^{\infty}\left|4kb_{n,k}\left[\frac{A_k}{4kb_{1,k}}\right]^n\sin(nk\theta+n\phi_k)\right|. \end{aligned} \tag{39}$$

The sine function and the factor $(4K)^{1-n}$ can be replaced by unity and we can bound the right-hand side of Eq. (39) by

$$\sum_{k=1}^{K}\sum_{n=2}^{\infty}\left[\frac{A_k}{b_{1,k}}\right]^n b_{n,k}\leqslant\sum_{k=1}^{K}A_k\sum_{n=1}^{\infty}\left[\frac{A_k}{b_{1,k}}\right]^n, \tag{40}$$

where we have used the fact that $b_{n,k}\leqslant b_{1,k}$, which follows directly from Eq. (36). Using now the facts that $b_{1,K}\leqslant b_{1,k}$ for every $k\leqslant K$ and A_k is bounded by some finite C since it is a Fourier coefficient, we can bound Eq. (40) by $C^2K/(b_{1,K}-C)$. Since we can select the free parameters Δ and M to make $b_{1,K}$ as large as we want, we can make the remainder series smaller in absolute value than $\epsilon/2$.

The conclusion of this demonstration is that any initial condition that can be represented in Fourier series can be approximated to a desired accuracy by pole decomposition. The number of needed poles is of the order K^2M. Of course, the number of poles thus generated by the initial conditions may exceed the number $N(L)$ found in Eq. (13). In such a case the excess poles will move to infinity and will become irrelevant for the short-time dynamics. Thus a smaller number of poles may be needed to describe the state at larger times than at $t=0$. We need to stress at this point that the pole decomposition is overcomplete; for example, if there is exactly one pole at $t=0$ and we use the above technique to reach a pole decomposition we would get a large number of poles in our representation.

B. Initial stages of the front evolution: The exponential stage and the inverse cascade

In this section we employ the connection between Fourier expansion and pole decomposition to understand the initial exponential stage of the evolution of the flame front with small initial data $u(\theta,t=0)$. Next we employ our knowledge of the pole interactions to explain the slow dynamics of coarsening into the steady-state solution.

Suppose that initially the expansion (29) is available with all the coefficients $A_k\ll 1$. We know from the linear instability of the flat flame front that each Fourier component changes exponentially in time according to the linear spectrum (6). The components with wave vector larger than Eq. (7) decrease, whereas those with lower wave vectors increase. The fastest growing mode is $k_c=L/2\nu$. In the linear stage of growth this mode will dominate the shape of the flame front, i.e.,

$$u(\theta,t)\approx A_{k_c}e^{\omega_{k_c}t}\sin(k_c\theta). \tag{41}$$

Using Eq. (34) for a large value of y (which is equivalent to small A_{k_c}) we see that to $O(A_{k_c}^2)$ Eq. (41) can be represented as a sum over $L/2\nu$ poles arranged periodically along the θ axis. Other unstable modes will contribute similar arrays of poles, but at much higher values of y since their amplitude is exponentially smaller. In addition, we have nonlinear corrections to the identification of the modes in terms of poles. These corrections can be again expanded in terms of Fourier modes and again identified with poles, which will be farther away along the y axis and with higher frequencies. To see this one can use Eq. (37), subtract from $u_p(\theta)$ the leading pole representations, and reexpand in a Fourier series. Then we identify the leading order with double the number of poles that are situated twice as far away along the y axis.

We note that even when all the unstable modes are present, the number of poles in the first-order identification is finite for finite L since there are only L/ν unstable modes. Counting the number of poles that each mode introduces, we get a total number of $(L/\nu)^2$ poles. The number $L/2\nu$ of poles that are associated with the most unstable mode is precisely the number allowed in the stable stationary solution; cf. Eq. (13). When the poles approach the real axis and cusps begin to develop, the linear analysis no longer holds, but the pole description does.

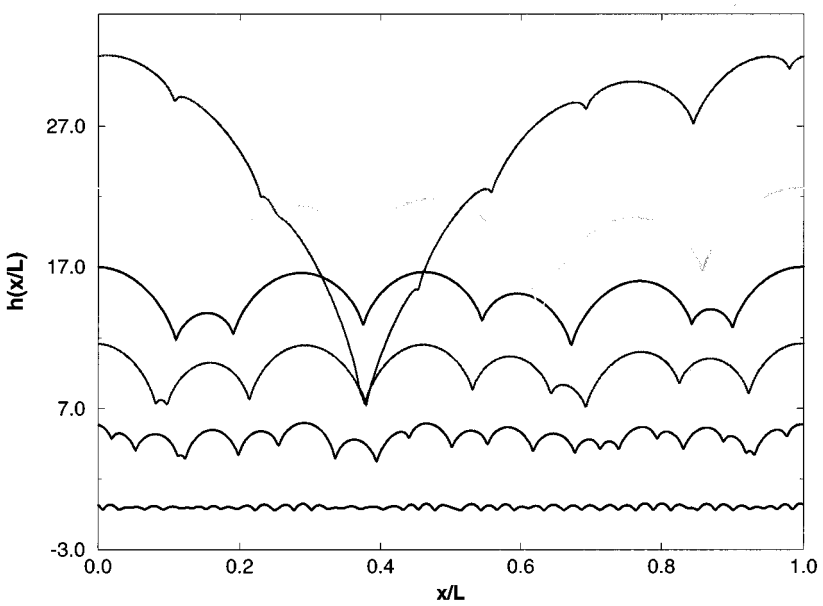

FIG. 3. Inverse cascade process of coarsening that occurs after preparing the system with random, small initial conditions. One sees that at successive times the typical scale increases until the giant cusp forms and attracts all the other side poles. The effect of the existing numerical additive noise is to introduce poles that appear as side cusps that are continuously attracted to the giant cusp. This effect is obvious to the eye only after the typical scale is sufficiently large, as is seen in the last time (see the text for further details).

We now describe the qualitative scenario for the establishment of the steady state. First, we understand that all the poles that belong to less unstable modes will be pushed towards infinity. To see this, think of the system at this stage as an array of uncoupled systems with a scale of the order of unity. Each such system will have a characteristic value of y. As we discussed before, poles that are farther away along the y axis will be pushed to infinity. Therefore the system will remain with the $L/2\nu$ poles of the most unstable mode. The net effect of the poles belonging to the (nonlinearly) stable modes is to destroy the otherwise perfect periodicity of the poles of the unstable mode. To see the effect of the higher-order correction to the pole identification we again recall that they can be represented as farther away poles with higher frequencies, whose dynamics is similar to the less unstable modes that were just discussed. They do not become more relevant when time goes on.

Once the poles of the stable modes get sufficiently far from the real axis, the dynamics of the remaining poles will begin to develop according to the interactions that are directed along the real axis. These interactions are much weaker and the resulting dynamics occur on much longer time scales. The qualitative picture is of an inverse cascade of merging the θ positions of the poles. We note that the system has a set of unstable fixed points that are ''cellular solutions'' described by a periodic arrangement of poles along the real axis with a frequency k. These fixed points are not stable and they collapse, under perturbations, with a characteristic time scale (which depends on k) to the next unstable fixed point at $k'=k/2$. This process then goes on indefinitely until $k\sim 1/L$, i.e., we reach the giant cusp, the steady-state stable solution [16].

This scenario is seen very clearly in the numerical simulations. In Fig. 3 we show the time evolution of the flame front starting from small white-noise initial conditions. The bottom curve pertains to the earliest time in this picture, just after the fast exponential growth, and one sees clearly the periodic array of cusps that form. The successive images show the progress of the flame front in time and one observes the development of larger scales with deeper cusps that represent the partial coalescence of poles onto the same θ positions. In Fig. 4 we show the width and the velocity of this front as a function of time. One recognizes the exponential stage of growth in which the $L/2\nu$ poles approach the θ axis and then a clear crossover to much slower dynamics in which the effective scale in the system grows with a slower rate.

The slow dynamics stage can be understood qualitatively using the previous interpretation of the cascade as follows: if the initial number of poles belonging to the unstable mode is $L/2\nu$, the initial effective linear scale is 2ν. Thus the first step of the inverse cascade will be completed in a time scale of the order of 2ν. At this point the effective linear scale doubles to 4ν and the second step will be completed after such a time scale. We want to know what the typical length scale l_t seen in the system at time t is. The typical width of the system at this stage will be proportional to this scale.

Denote the number of cascade steps that took place until this scale is achieved by s_l. The total time elapsed $t(l_t)$ is the sum

$$t(l_t)\sim\sum_{i=1}^{s_l} 2^i. \tag{42}$$

The geometric sum is dominated by the largest term and we therefore estimate $t(l_t)\sim l_t$. We conclude that the scale and the width are linear in the time elapsed from the initial conditions ($l_t\sim t^{\zeta}, \zeta=1$). In noiseless simulations we find (see Fig. 4) a value of ζ that is $\zeta\approx 0.95\pm 0.1$.

C. Inverse cascade in the presence of noise

An interesting consequence of the discussion in the preceding subsection is that the inverse cascade process is an effective ''clock'' that measures the typical time scales in this system. For future purposes we need to know the typical time scales when the dynamics is perturbed by random noise. To this aim we ran simulations following the inverse cascade in the *presence* of external noise. The main result that will be used in later arguments is that now the appearance of a typical scale l_t occurs not after time t, but rather according to

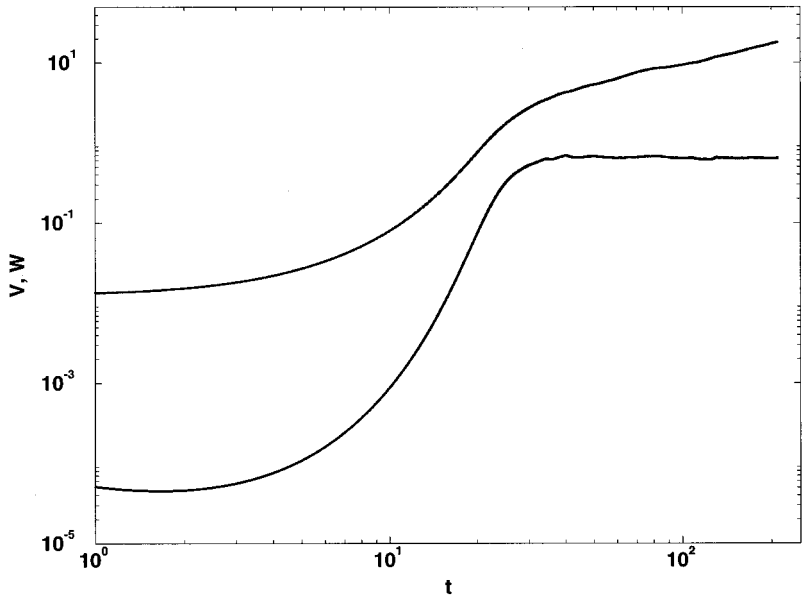

FIG. 4. Log-log plots of the front velocity (lower curve) and width (upper curve) as a function of time in the inverse cascade process seen in Fig. 3 in a system of size 2000 and $\nu=1$. Both quantities exhibit an initial exponential growth that turns to a power-law growth (after $t\approx 30$). The velocity is constant after this time and the width increases like t^{ζ}. Note that at the earliest time there is a slight decrease in the velocity; this is due to the decay of linearly stable modes that exist in random initial conditions.

$$l_t \sim t^{\zeta}, \quad \zeta \approx 1.2 \pm 0.1. \tag{43}$$

The numerical confirmation of this law is exhibited in Fig. 5. We also find that the front velocity in this case increases with time according to

$$v \sim t^{\gamma}, \quad \gamma \approx 0.48 \pm 0.05. \tag{44}$$

This result will be related to the acceleration of the flame front in noisy simulations, as will be seen in the following sections. The result (43) will be helpful in Sec. VC in estimating the values of the scaling exponents.

V. ACCELERATION OF THE FLAME FRONT, POLE DYNAMICS, AND NOISE

A major motivation of this section is the observation that in radial geometry the same equation of motion shows an acceleration of the flame front. The aim of this section is to argue that this phenomenon is caused by the noisy generation of new poles. Moreover, it is our contention that a great deal can be learned about the acceleration in radial geometry by considering the effect of noise in channel growth. In Ref. [9] it was shown that any initial condition that is represented in poles goes to a unique stationary state that is the giant cusp that propagates with a constant velocity $v=1/2$ up to small $1/L$ corrections. In light of our discussion of the preceding section, we expect that any smooth enough initial condition will go to the same stationary state. Thus if there is no noise in the dynamics of a finite channel, no acceleration of the flame front is possible. What happens if we add noise to the system?

For concreteness we introduce an additive white-noise term $\eta(\theta,t)$ to the equation of motion (5) where

$$\eta(\theta,t)=\sum_k \eta_k(t)\exp(ik\theta) \tag{45}$$

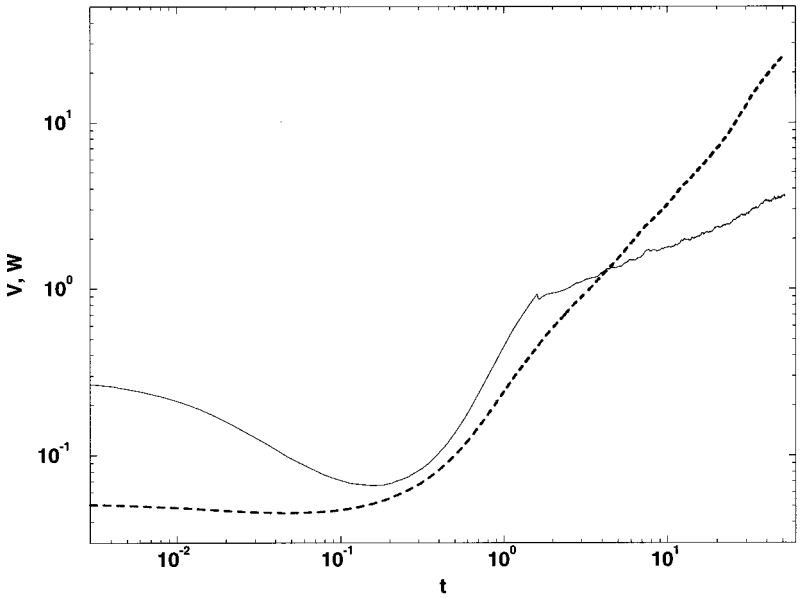

FIG. 5. The same as Fig. 4, but with additive random noise for a system of size 1000, $\nu=0.1$, and $f=10^{-13}$. The velocity does not saturate now and the exponent ζ characterizing the increase of the width with time changes to $\zeta=1.2\pm 0.1$. The velocity increases in time like t^{γ} with $\gamma\approx 0.48\pm 0.04$.

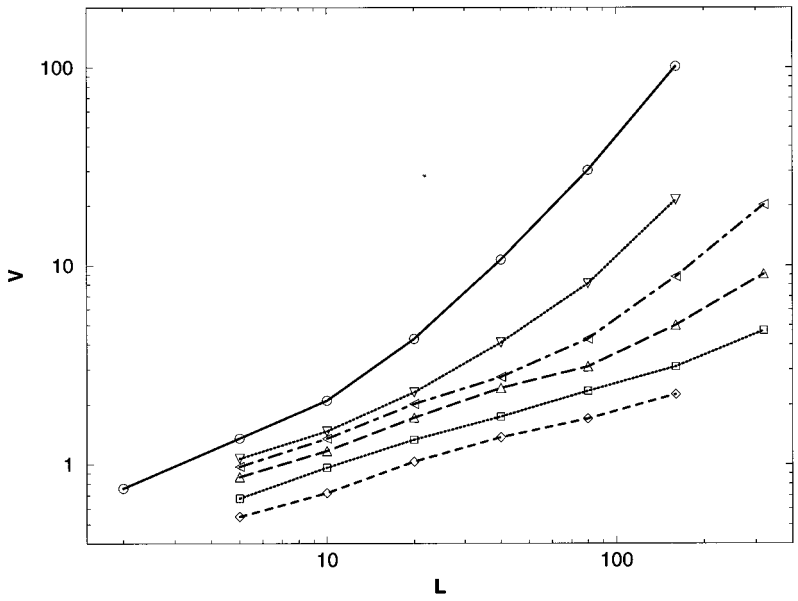

FIG. 6. Log-log plot of the velocity as a function of system size for different values of the noise amplitude $\sqrt{f}=2.5\times10^{-13}$, 2.5×10^{-9}, 2.5×10^{-7}, 10^{-6}, 4×10^{-6}, and $2.5\times10^{-5}$and $\nu=0.1$. For low values of f we observe a power-law behavior $v\sim L^{\mu}$, $\mu\approx0.42\pm0.03$. For larger values of f there is a crossover to a stronger dependence on the system size; see the text for details.

and the Fourier amplitudes η_k are correlated according to

$$\langle \eta_k(t)\,\eta^*_{k'}(t')\rangle = f\,\delta(k-k')\,\delta(t-t'). \tag{46}$$

We will first examine the result of numerical simulations of noise-driven dynamics and later return to the theoretical analysis.

A. Noisy simulations

Previous numerical investigations [6,15] did not introduce noise in a controlled fashion. We will argue later that some of the phenomena encountered in these simulations can be ascribed to the (uncontrolled) numerical noise. We performed numerical simulations of Eq. (5) using a pseudospectral method. The Adams-Bashforth time-stepping scheme was chosen with second-order precision in time. The additive white noise was generated in Fourier space by choosing η_k for every k from a flat distribution in the interval $[-\sqrt{2f},\sqrt{2f}]$. We examined the average steady-state velocity of the front as a function of L for fixed f and as a function of f for fixed L. We found the interesting phenomena that are summarized here.

(i) When the noise level f is fixed the average velocity v increases with L; see Fig. 6. There are two different regimes of this behavior. For sufficiently small values of f and L we observe a power law dependence of v on L:

$$v\sim L^{\mu}, \quad \mu\approx0.42\pm0.03. \tag{47}$$

For large values of f and L the dependence of v on L is much stronger, $\mu>1.5$, but we cannot estimate it well because of a lack of dynamical range. For a given value of f the transition between the two regimes appears upon increasing L and we denote the critical value as $L_c(f)$; see Fig. 7. The data indicate that

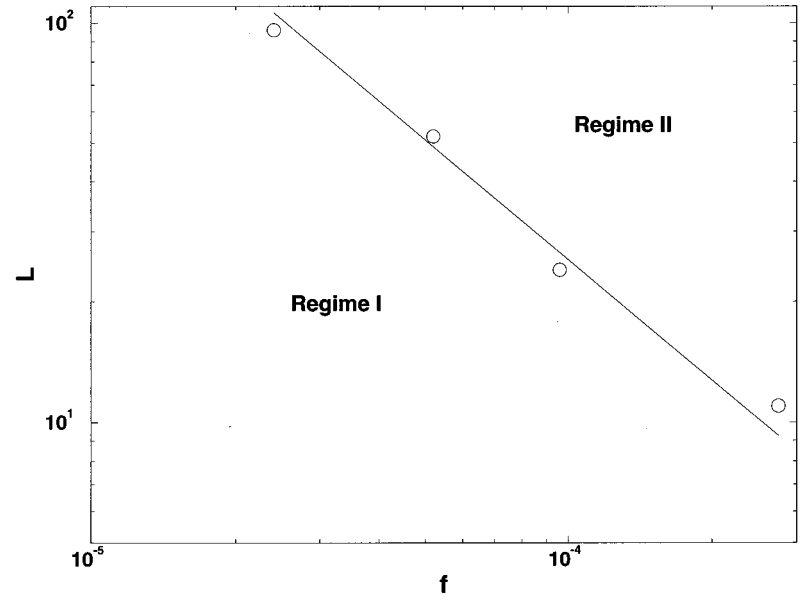

FIG. 7. Critical value of L as a function of f for which the transition from weaker to stronger dependence of v on L is observed; see Fig. 6. In regime I the noise is relatively small and the cusp picture is qualitatively correct. In regime II the noise is too large to leave the cusp picture intact; see the text and Figs. 9 and 10 for further details. The data indicate a power law as explained in the text.

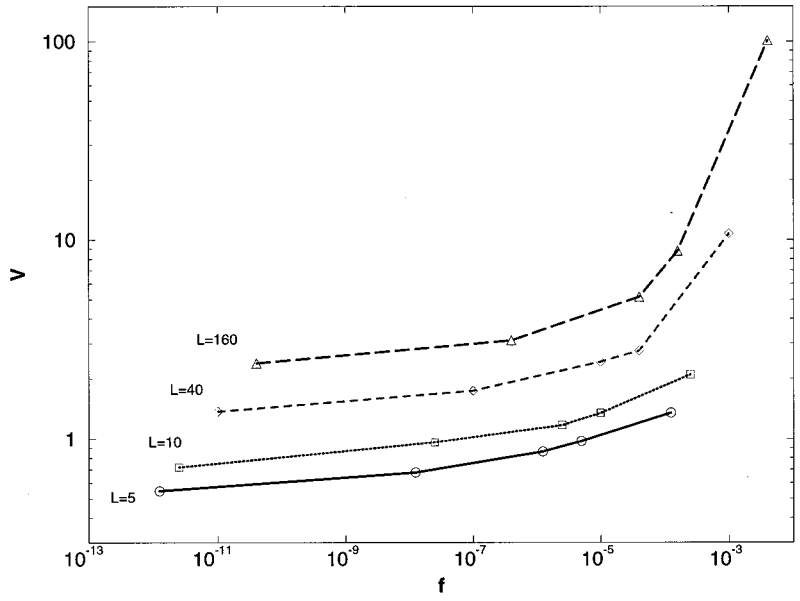

FIG. 8. Log-log plot of the velocity vs the noise amplitude for different system sizes $\tilde{L}=5$, 10, 40, and 160 and $\nu=0.1$.

$$L_c(f)\sim f^{-\alpha}, \tag{48}$$

with $\alpha\approx 1.0\pm 0.2$.

(ii) When the system size L is fixed the average velocity depends on f as

$$v\sim f^{\xi}. \tag{49}$$

For sufficiently small value of f this dependence is very weak and $\xi\approx 0.02$; see Fig. 8. For large values of f the dependence is much stronger, $\xi=1\pm 0.1$.

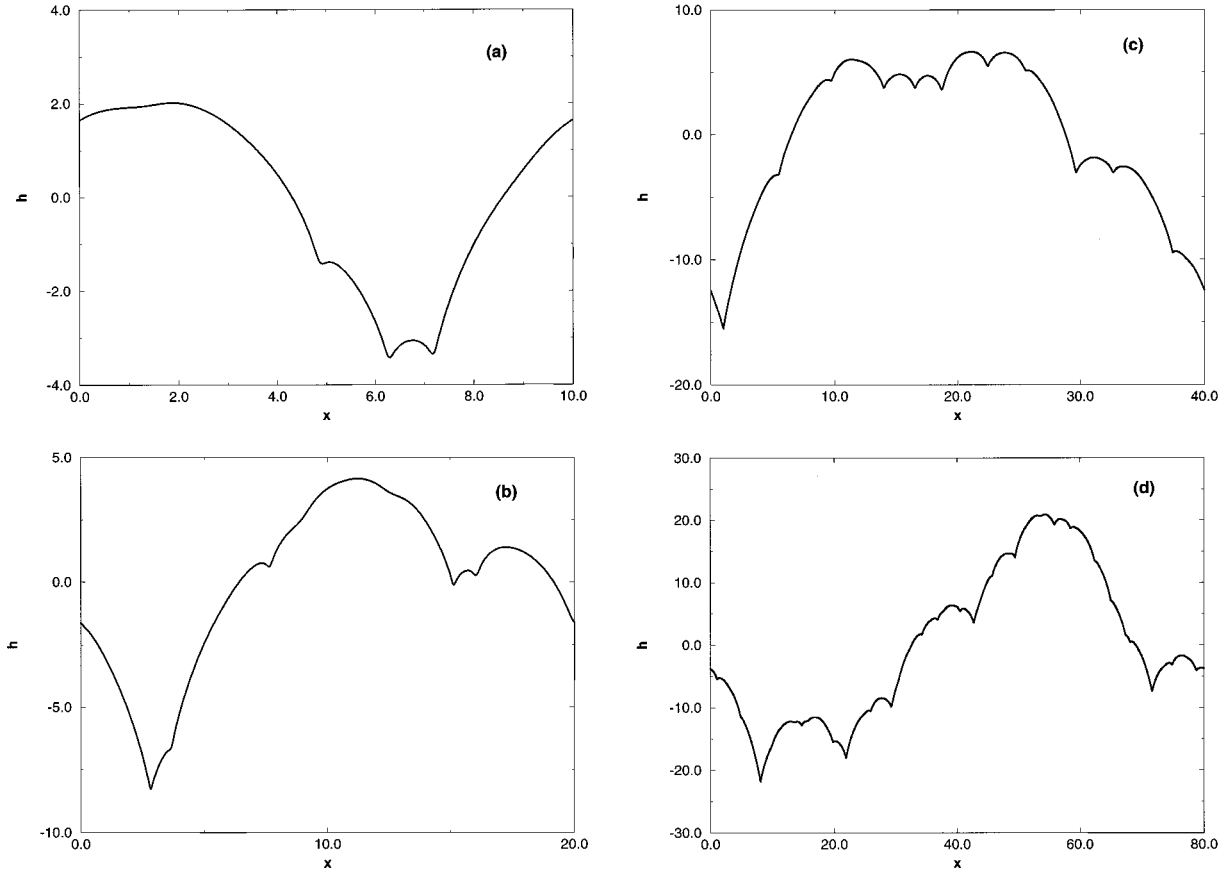

FIG. 9. Typical flame fronts in regime I of Fig. 7, where the system is sufficiently small not to be terribly affected by the noise. The effect of noise in this regime is to add additional small cusps to the giant cusp. In (a)–(d) we present fronts for growing system sizes $\tilde{L}=10,\ 20,\ 40$, and 80, respectively, $\nu=0.1$, and $\sqrt{f}=2.5\times 10^{-9}$. One can observe that when the system size grows there are more cusps with a more complex structure.

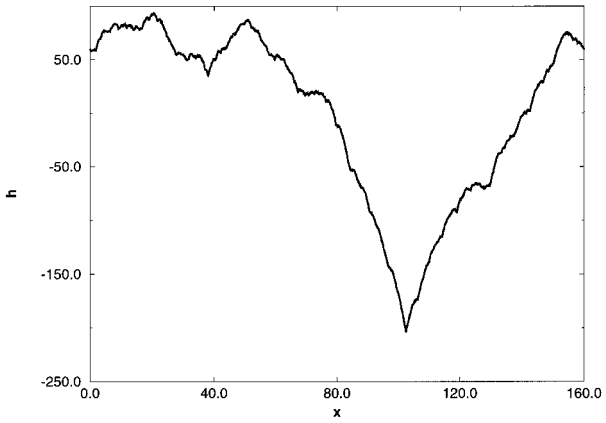

FIG. 10. Typical flame front in regime II of Fig. 7. The system size is 160 and the noise amplitude is 2.5×10^{-5}. This is sufficient to cause a qualitative change in the appearance of the flame front: the noise introduces significant levels of small scales structure in addition to the cusps.

(iii) The locus separating weaker dependences of v on L and f (regime I) from stronger dependences (regime II) is shown in Fig. 7. The giant cusp remains recognizable in both regimes. In regime I one observes a series of small cusps superposed on the structure of the giant cusp. In Fig. 9 we show a set of interfaces with a growing size and with the same noise. One can observe a strong increase in the number of cusps and the complexity of their arrangements as the system size increases. In regime II there are strong fluctuations in the gradient field $u(\theta,t)$; see Fig. 10.

(iv) Measurements of the width of the front indicate that it has a a very weak dependence on f for fixed L in regime I.

B. Theoretical discussion of the effect of noise

1. Threshold of instability to added noise

First we present the theoretical arguments that explain the sensitivity of the giant cusp solution to the effect of added noise. This sensitivity increases dramatically with increasing the system size L. To see this we use again the relationship between the linear stability analysis and the pole dynamics.

Our additive noise introduces perturbations with all k vectors. We showed previously that the most unstable mode is the $k=1$ component $A_1\sin(\theta)$. Thus the most effective noisy perturbation is $\eta_1\sin(\theta)$, which can potentially lead to a growth of the most unstable mode. Whether or not this mode will grow depends on the amplitude of the noise. To see this clearly we return to the pole description. For small values of the amplitude A_1 we represent $A_1\sin(\theta)$ as a single pole solution of the functional form $\nu e^{-y}\sin\theta$. The y position is determined from $y=-\ln|A_1|/\nu$ and the θ position is $\theta=\pi$ for positive A_1 and $\theta=0$ for negative A_1. From the analysis of Sec. III we know that for very small A_1 the fate of the pole is to be pushed to infinity, independently of its θ position; the dynamics is symmetric in $A_1\to-A_1$ when y is large enough. On the other hand, when the value of A_1 increases the symmetry is broken and the θ position and the sign of A_1 become very important. If $A_1>0$ there is a threshold value of y below which the pole is attracted down. On the other hand, if $A_1<0$ and $\theta=0$ the repulsion from the poles of the giant cusp grows with decreasing y. We thus understand that, qualitatively speaking, the dynamics of A_1 is characterized by an asymmetric ''potential'' according to

$$\dot{A}_1=-\frac{\partial V(A_1)}{\partial A_1}, \tag{50}$$

$$V(A_1)=\lambda A_1^2-aA_1^3+\cdots. \tag{51}$$

From the linear stability analysis we know that $\lambda\approx\nu/L^2$; cf. Eq. (14). We know further that the threshold for nonlinear instability is at $A_1\approx\nu^3/L^2$; cf. Eq. (28). This determines that value of the coefficient $a\approx2/3\nu^2$. The magnitude of the potential at the maximum is

$$V(A_{\max})\approx\nu^7/L^6. \tag{52}$$

The effect of the noise on the development of the mode $A_1\sin\theta$ can be understood from the stochastic equation

$$\dot{A}_1=-\frac{\partial V(A_1)}{\partial A_1}+\eta_1(t). \tag{53}$$

It is well known [17] that for such dynamics the rate of escape R over the potential barrier for small noise is proportional to

$$R\sim\frac{\nu}{L^2}\exp(-\nu^7/fL^6). \tag{54}$$

The conclusion is that any arbitrarily tiny noise becomes effective when the system size increases and when ν decreases. If we drive the system with noise of amplitude f the system can always be sensitive to this noise when its size exceeds a critical value L_c, which is determined by $f\sim\nu^7/L_c^6$. For $L>L_c$ the noise will introduce new poles into the system. Even numerical noise in simulations involving large size systems may have a macroscopic influence.

The appearance of new poles must increase the velocity of the front. The velocity is proportional to the mean of $(u/L)^2$. New poles distort the giant cusp by additional smaller cusps on the wings of the giant cusp, increasing u^2. Upon increasing the noise amplitude more and more smaller cusps appear in the front and inevitably the velocity increases. This phenomenon is discussed quantitatively in Sec. V.

2. The noisy steady state and its collapse with large noise and system size

In this subsection we discuss the response of the giant cusp solution to noise levels that are able to introduce a large number of excess poles in addition to those existing in the giant cusp. We will denote the excess number of poles by δN. The first question that we address is how difficult it is to insert yet an additional pole when there is already a given excess δN. To this aim we estimate the effective potential $V_{\delta N}(A_1)$, which is similar to Eq. (51), but takes into account the existence of an excess number of poles. A basic approximation that we employ is that the fundamental form of the giant cusp solution is not seriously modified by the existence of an excess number of poles. Of course, this approximation

breaks down quantitatively already with one excess pole. Qualitatively, however, it holds well until the excess number of poles is of the order of the original number $N(L)$ of the giant cusp solution. Another approximation is that the rest of the linear modes play no role in this case. At this point we limit the discussion, therefore, to the situation $\delta N \ll N(L)$.

To estimate the parameter λ in the effective potential we consider the dynamics of one pole whose y position y_a is far above $y_{\max}$. According to Eq. (14), the dynamics reads

$$\frac{dy_a}{dt} \approx \frac{2\nu[N(L)+\delta N]}{L^2} - \frac{1}{L}. \tag{55}$$

Since the $N(L)$ term cancels against the L^{-1} term (cf. Sec. II A), we remain with a repulsive term that in the effective potential translates to

$$\lambda = \frac{\nu \delta N}{L^2}. \tag{56}$$

Next we estimate the value of the potential at the break-even point between attraction and repulsion. In Sec. V B 1 we saw that a foreign pole has to be inserted below $y_{\max}$ in order to be attracted towards the real axis. Now we need to push the new pole below the position of the existing pole whose index is $N(L)-\delta N$. This position is estimated as in Sec. III C by employing the TFH distribution function (25). We find

$$y_{\delta N} \approx 2 \ln\left[\frac{4L}{\pi^2 \nu \delta N}\right]. \tag{57}$$

As before, this implies a threshold value of the amplitude of single pole solution $A_{\max}\sin\theta$ that is obtained from equating $A_{\max} = \nu e^{y_{\delta N}}$. We thus find in the present case $A_{\max} \sim \nu^3 (\delta N)^2 / L^2$. Using again a cubic representation for the effective potential we find $a = 2/3\,\nu^2 \delta N$ and

$$V(A_{\max}) = \frac{1}{3}\frac{\nu^7 (\delta N)^5}{L^6}. \tag{58}$$

Repeating the calculation of the escape rate over the potential barrier, we find in the present case

$$R \sim \frac{\nu \delta N}{L^2} \exp[-\nu^7 (\delta N)^5 / f L^6]. \tag{59}$$

For a given noise amplitude f there is always a value of L and ν for which the escape rate is of $O(1)$ as long as δN is not too large. When δN increases the escape rate decreases, and eventually no additional poles can creep into the system. The typical number δN for fixed values of the parameters is estimated from equating the argument in the exponent to unity

$$\delta N \approx (f L^6 / \nu^7)^{1/5}. \tag{60}$$

The most important consequence of this relation is that δN increases with L faster than $N(L)$. Accordingly, we expect a breakdown of this picture and of the weak-noise behavior when $\delta N \approx N(L)$, which occurs when L reaches a critical value $L_c(f)$, where

$$L_c(f) \sim f^{-1}. \tag{61}$$

This prediction is in good quantitative agreement with Eq. (48), supporting the analytical theory.

C. Acceleration of the flame front due to noise

In this section we estimate the scaling exponents that characterize the velocity of the flame front as a function of the system size. Our arguments in this section are even less solid than the previous ones, but, nevertheless, we believe that we succeed in capturing some of the essential qualitative physics that underlies the interaction between noise and instability and results in the acceleration of the flame front.

To estimate the velocity of the flame front we need to write down an equation for the mean of $\langle dh/dt \rangle$ given an arbitrary number N of poles in the system. This equation follows directly from Eq. (4):

$$\left\langle \frac{dh}{dt} \right\rangle = \frac{1}{L^2}\frac{1}{2\pi}\int_0^{2\pi} u^2 d\theta. \tag{62}$$

After substitution of Eq. (8) in Eq. (62) we get, using Eqs. (11) and (12),

$$\left\langle \frac{dh}{dt} \right\rangle = 2\nu \sum_{k=1}^{N} \frac{dy_k}{dt} + 2\left\langle \frac{\nu N}{L} - \frac{\nu^2 N^2}{L^2} \right\rangle. \tag{63}$$

The estimates of the second and third terms in this equation are straightforward. Writing $N = N(L) + \delta N(L)$ and remembering that $N(L) = \nu/L$, we find that these terms contribute $-\nu \delta N(L)/L \sim -L^{1/5}$. The first term will contribute only when the current of poles is asymmetric. Since noise introduces poles at a finite value of y, whereas the rejected poles stream towards infinity, we have an asymmetry that contributes to the velocity of the front. To estimate the first term we remind the reader of our discussion in Sec. IV C. In this problem the typical time scale for the poles is the coalescense time of poles with an initial distance L in the x direction. In noiseless conditions the typical time scales like L. In the presence of noise [cf. Eq. (43)] we found numerically in Sec. IV C that it scales like $L^{1/\zeta}$. Accordingly, the typical flux of poles can be estimated as $\delta N(L)/L^{1/\zeta}$. Thus the current $\Sigma \dot{y}_k$ has a stronger dependence on L, i.e., $L^{6/5-1/\zeta}$. Taking the numerical value of $\zeta = 1.2$ we conclude that Eq. (63) predicts a scaling law (47) with $\mu = 0.37$, in reasonable agreement with the numerics.

We should stress at this point that the argument is not complete. First, we used the inverse cascade measurement to invoke a typical time scale for the coalescence of poles by motion along the x axis when the distance between them is L, and we used this time scale for the coalescence of poles in a system whose integral scale is L. This can be taken only as a lower bound of the exponent characterizing the time scale beacuse of the intervention of additional modes in the larger system. The simple identification is a sort of ''single-mode'' approximation in which the dynamics is carried by the most unstable mode only. Second, we measured the exponent relating the velocity to the amplitude of external noise [cf. Eq. (49)] and found that ξ is considerably smaller than the value 1/5, which is predicted by the previous argument. This indi-

cates that the typical time scale also has an explicit f dependence that is physically plausible, but it was not measured in our simulations.

VI. SUMMARY AND CONCLUSIONS

The two main messages of this paper are that (i) there is an important interaction between the instability of developing fronts and random noise and (ii) this interaction and its implications can be understood qualitatively and sometimes quantitatively using the description in terms of complex poles. The pole description is natural in this context, first because it provides an exact (and effective) representation of the steady state without noise. Once one succeeds in describing also the *perturbations* about this steady state in terms of poles, one achieves a particularly transparent language for the study of the interplay between noise and instability. This language also allows us to describe in qualitative and semiquantitative terms the inverse cascade process of increasing typical lengths when the system relaxes to the steady state from small, random initial conditions.

The main conceptual steps in this paper are as follows. First, one realizes that the steady-state solution, which is characterized by $N(L)$ poles aligned along the imaginary axis, is marginally stable against noise in a periodic array of L values. For all values of L the steady state is nonlinearly unstable against noise. The main and foremost effect of noise of a given amplitude f is to introduce an excess number of poles $\delta N(L,f)$ into the system. The existence of this excess number of poles is responsible for the additional wrinkling of the flame front on top of the giant cusp and for the observed acceleration of the flame front. By considering the noisy appearance of new poles we rationalize the observed scaling laws as a function of the noise amplitude and the system size.

Theoretically, we therefore concentrate on estimating $\delta N(L,f)$. The measurements do not test our theoretical consideration directly, but rather test the dependence of the velocity on L and f. The only direct test for our theory is the critical line shown in Fig. 7. The measured exponent is in accord with our analytic estimates. Nevertheless, we note that some of our considerations are only qualitative. For example, we estimated $\delta N(L,f)$ by assuming that the giant cusp solution is not seriously perturbed. On the other hand, we find a flux of poles going to infinity due to the introduction of poles at finite values of y by the noise. The existence of poles spread between $y_{\max}$ and infinity *is* a significant perturbation of the giant cusp solution. Thus also the comparison between the various scaling exponents measured and predicted must be done with caution; we cannot guarantee that those cases in which our prediction hits close to the measurement mean the theory is quantitative. However, we believe that our consideration extracts the essential ingredients of a correct theory.

The ''phase diagram'' as a function of L and f in this system consists of three regimes. In the first one, discussed in Sec. V B 1, the noise is too small to have any effect on the giant cusp solution. In the second the noise introduces excess poles that serve to decorate the giant cusp with side cusps. In this regime we find scaling laws for the velocity as a function of L and f and we are reasonably successful in understanding the scaling exponents. In the third regime the noise is large enough to create small-scale structures that are not neatly understood in terms of individual poles. It appears from our numerics that in this regime the roughening of the flame front gains a contribution from the small-scale structure in a way that is reminiscent of *stable*, noise driven growth models such as the Kardar-Parisi-Zhang model.

One of our main motivations in this research was to understand the phenomena observed in radial geometry with expanding flame fronts. A full analysis of this problem cannot be presented here. We note, however, that many of the insights offered above translate immediately to that problem. Indeed, in radial geometry the flame front accelerates and cusps multiply and form a hierarchic structure as time progresses. Since the radius (and the typical scale) increase in this system all the time, new poles will be added to the system even by a vanishingly small noise. The marginal stability found above holds also in this case and the system will allow the introduction of excess poles as a result of noise. The results discussed in Ref. [7] can be combined with the present insights to provide a theory of radial growth. This theory will be offered in a forthcoming paper.

Finally, the success of this approach in the case of flame propagation raises hope that Laplacian growth patterns may be dealt with using similar ideas. A problem of immediate interest is Laplacian growth in channels, in which a finger steady-state solution is known to exist. It is documented that the stability of such a finger solution to noise decreases rapidly with increasing the channel width. In addition, it is understood that noise brings about additional geometric features on top of the finger. There are enough similarities here to indicate that a careful analysis of the analytic theory may shed as much light on that problem as on the present one.

ACKNOWLEDGMENTS

This work was supported in part by the German Israeli Foundation, the U.S.–Israel Binational Science Foundation, the Minerva Center for Nonlinear Physics, and the Naftali and Anna Backenroth-Bronicki Fund for Research in Chaos and Complexity.

[1] P. Pelce, *Dynamics of Curved Fronts* (Academic, Boston, 1988).

[2] A.-L. Barbási and H.E. Stanley, *Fractal Concepts in Surface Growth* (Cambridge University Press, Cambridge, 1995).

[3] T. Viscek, *Fractal Growth Phenomena* (World Scientific, Singapore, 1992).

[4] G.I. Sivashinsky, Acta Astronaut. **4**, 1177 (1977).

[5] Yu.A. Gostintsev, A.G. Istratov, and Yu.V. Shulenin, Com-

bust. Expl. Shock Waves **24**, 70 (1989).
[6] L. Filyand, G.I. Sivahshinsky, and M.L. Frankel, Physica D **72**, 110 (1994).
[7] O. Kupervasser, Z. Olami, and I. Procaccia, Phys. Rev. Lett. **76**, 146 (1996).
[8] Y.-C. Lee and H.H. Chen, Phys. Scr. **T2**, 41 (1982).
[9] O. Thual, U. Frisch, and M. Hénon, J. Phys. (Paris) **46**, 1485 (1985).
[10] G. Joulin, J. Phys. (Paris) **50**, 1069 (1989).
[11] G. Joulin, Zh. Éksp. Teor. Fiz. **100**, 428 (1990).
[12] B.I. Shraiman and D. Bensimon, Phys. Rev. A **30**, 2840 (1984).
[13] S.D. Howison, J. Fluid Mech. **167**, 439 (1986).
[14] S. Ponce Dawson and M. Mineev-Weinstein, Physica D **73**, 373 (1994).
[15] S. Gutman and G. I. Sivashinsky, Physica D **43**, 129 (1990).
[16] See, for example, B. Galanti, P.L. Sulem, and A.D. Gilbert, Physica D **47**, 416 (1991), and references cited therein.
[17] H. Risken, *The Fokker-Planck Equation* (Springer, Berlin, 1984), p. 124, Eq. (5.111).